The Role of Surface-Capping Ligands in Photoexcited Electron Transfer between CdS Nanorods and [FeFe] Hydrogenase and the subsequent $\rm H_2$ Generation

Molly B. Wilker, † Sophie Greene, † Katherine A. Brown, David W.

Mulder, [‡] Paul W. King, [‡] Gordana Dukovic*, [†]

[†]Department of Chemistry and Biochemistry, University of Colorado Boulder, Boulder,

Colorado 80309, United States

*Biosciences Center, National Renewable Energy Laboratory, Golden, Colorado 80401, United States

ABSTRACT

Complexes of CdS nanorods and [FeFe] hydrogenase from *Clostridium acetobutylicum* have been shown to photochemically produce H₂. This study examines the role of the ligands that passivate the nanocrystal surfaces in the electron transfer from photoexcited CdS to hydrogenase and the H₂ generation that follows. We functionalized CdS nanorods with a series of mercaptocarboxylate surface-capping ligands of varying lengths and measured their photoexcited electron relaxation by transient absorption (TA) spectroscopy before and after hydrogenase adsorption. Rate constants for electron transfer from the nanocrystals to the enzyme, extracted by modeling of TA kinetics, decrease exponentially with ligand length, suggesting that the ligand layer acts as a barrier to charge transfer and controls the degree of electronic coupling. Relative light-driven H₂ production efficiencies follow the relative quantum efficiencies of electron transfer, revealing the critical role of surface-capping ligands in determining the photochemical activity of these nanocrystal-enzyme complexes. Our results suggest that the H₂ production in this system could be maximized with a choice of a surface-capping ligand that decreases the distance between the nanocrystal surface and the electron injection site of the enzyme.

1. INTRODUCTION

Architectures that couple cadmium chalcogenide nanocrystals with redox enzymes have emerged as an intriguing strategy to use light to drive multi-electron redox reactions such as proton reduction to H₂, CO₂ reduction to CO, and N₂ fixation to NH₃.¹⁻¹² These systems all operate on a similar general principle: light absorption in the nanocrystal is followed by electron transfer (ET) to the enzyme, which stores and uses the electrons for the multi-electron reduction reaction. Holes are scavenged by sacrificial electron donors, most frequently ascorbate. Because the electrons in the final photochemical product arrive from the nanocrystals, the kinetics of the

ET step play a critical role in the overall photochemistry, as we showed in the example of CdS nanorods (NRs) and an [FeFe] hydrogenase (H₂ase).^{7,8} In particular, ET competes with electronhole recombination and electron trapping in the nanocrystal. The interplay of the rates for these processes determines quantum efficiency of ET (QE_{ET}), which in turn defines the upper limit of the overall photochemical efficiency.^{7,8,13} In the CdS–H₂ase system, QE_{ET} depends strongly on the ratio of the ET and recombination rate constants such that an order of magnitude change in either variable can alter the end result dramatically.⁸ As this example illustrates, understanding the factors that govern the kinetics of ET and the competing processes in the nanocrystal is critical to controlling light-driven redox chemistry of nanocrystal-enzyme complexes.

In nanocrystal-enzyme architectures in general, and the CdS–H₂ase system in particular, the interface between the light absorber and the catalyst is determined by the capping ligands on the nanocrystal surface. Evidence suggests that CdS–H₂ase complexes form via an electrostatic interaction in which CdS NRs, capped with negatively-charged mercaptopropionate ligands, bind to a positively charged region on H₂ase.^{1,2,6-8} This biomimetic interaction is analogous to the binding of ferredoxin, the natural electron donor partner of H₂ase,^{1,2} allowing the electrons from the nanocrystals to be injected at the same iron-sulfur cluster in both cases.^{7,14} The surface-capping ligands may play multiple roles in ET and the overall photochemistry. They enable the solubility of complexes in aqueous buffer and facilitate the electrostatic nanocrystal-enzyme binding via the negative carboxylate groups. Surface-capping ligands also affect the competing relaxation pathways, especially the electron trapping on the nanocrystal surface.¹⁵ Finally, our working model of the nanocrystal-enzyme interaction suggests that the ligands impact the electronic coupling between CdS and the electron injection site of H₂ase.

In this work, we examine how surface-capping ligands on CdS NRs impact ET kinetics and photochemical H₂-production rates. Specifically, we use a sequence of mercaptocarboxylate ligands with varying aliphatic chain lengths while keeping the ligand functional groups that govern the interactions between the nanocrystal and the enzyme constant. To determine the ET rates in each CdS–H₂ase system, we measured the relaxation dynamics of photoexcited electrons in CdS NRs with and without H₂ase using transient absorption (TA) spectroscopy. We analyzed the data using a kinetic model that allowed us to extract the rate constants for electron-hole recombination, electron trapping, ET, and the average number of enzymes adsorbed, all of which were ligand-dependent. Each sample of CdS NRs capped with a ligand of different length

exhibited slightly different photoexcited electron decay kinetics due to the impact of ligands on nanocrystal photophysics. Once mixed with H₂ase, the number of enzymes adsorbed also varied with ligand length. Most notably, the rate constant of ET decreased exponentially with increasing ligand length. This strong dependence suggests that the surface-capping ligands form a bridge between the nanocrystal donor and the enzyme acceptor, consistent with our model of the nanocrystal-enzyme interaction.² Similar to other nanocrystal-acceptor systems, ¹⁶⁻²⁵ the ligand acts as a bridge with weak electronic coupling that falls off rapidly with distance. We also report a significant decrease in the quantity of photogenerated H₂ as the length of the nanocrystal surface ligand increases. By comparing QE_{ET} with H₂ production, we show that, although not the only factor that determines H₂ production, the competitiveness of ET with the other electron relaxation processes plays a governing role in the photocatalytic efficiency of this system. This, in turn, suggests that ET efficiency could be controlled with judicious choice of surface-capping ligands that enhance both the electronic coupling and enzyme adsorption.

2. METHODS

2.1 Nanocrystal Preparation. The CdS NRs synthesis was adapted from a published procedure for a seeded-growth method and carried out in an argon atmosphere. CdS seeds were synthesized from an initial mixture of 0.100 g cadmium oxide (CdO, 99.99% Aldrich), 0.603 g octadecylphosphonic acid (ODPA, 99%, PCI Synthesis), and 3.299 g trioctylphosphine oxide (TOPO, 99%, Aldrich). At 320°C, a sulfur stock solution (0.179 g hexamethyldisilathiane ((TMS)₂S, synthesis grade, Aldrich) in 3 g of tributylphosphine (TBP, 97%, Aldrich)) was quickly injected. Nanocrystal growth proceeded for 7.5 minutes at 250°C. The reaction was stopped by removing the heating mantle and injecting 4 mL of anhydrous toluene. The CdS seeds were washed by precipitation with methanol and the final product was dissolved in trioctylphosphine (TOP, 97%, Strem). The CdS seeds had their lowest-energy exciton peak at 408 nm. The rods were synthesized from a starting solution of 0.086 g CdO, 3 g TOPO, 0.290 g ODPA, and 0.080 g hexylphosphonic acid (HPA, 99%, PCI Synthesis). The solution was heated to 350°C then 1.5 mL of TOP was injected into the solution. When the temperature of the Cd-containing solution stabilized at 350°C, the seed-containing sulfur injection solution (0.124 g of sulfur (S, 99.998%, Aldrich) in 1.5 mL of TOP mixed with 8 × 10⁻⁸ mol CdS OD seeds) was

quickly injected. Nanocrystal growth proceeded for 8 minutes, after which the solution was cooled and the particles were purified using size-selective precipitation

The resulting NRs had average diameters of 3.7 ± 0.3 nm and an average length of 22.6 ± 1.8 nm as determined by measurements of 300 particles in transmission electron microscopy (TEM) images. The molar absorptivity (ε) of the CdS NRs was determined by correlating absorption spectra with Cd²⁺ concentrations determined by elemental analysis (ICP-OES). The estimated value of ε_{350} was 1710 M⁻¹ cm⁻¹ per Cd²⁺. The number of Cd²⁺ per NR was estimated from the average NR dimensions. ε_{350} was 8.6 x 10⁶ M⁻¹ cm⁻¹. The hydrophobic surface-capping ligands on the as-synthesized CdS NRs were replaced with mercaptocarboxylate ligands following the previously reported procedure, and the resulting particles were redispersed in 12.5 mM Tris buffer, pH 7.²

The length of each ligand, defined as the distance between the center of the S atom to the center of the furthest O atom in the carboxylate, was estimated based on alkyl chain C-C bond lengths of 1.523 Å, C-C bond lengths of 1.509 Å for the carboxylate carbon, carboxylate C-O bond lengths of 1.250 Å, C-S bond lengths of 1.815 Å, C-C-C and C-C-S bond angles of 109.5°, and carboxylate C-C-O bond angles of 120°.

2.2 H_2 ase Purification, Characterization, and Coupling to CdS NRs. The [FeFe] hydrogenase from *Clostridium acetobutylicum* (CaI) was expressed and purified from *Escherichia coli* as previously described with some modifications.²⁷ For expression, cells were grown in a 10 L fermenter (Sartorius Stedim Biotech) at 37°C with 250 rpm stirring and 0.9 L/min air bubbling. For induction, 1.5 mM Isopropyl β -D-1-thiogalactopyranoside (IPTG) was added, along with 4 mM ammonium iron (III) citrate, 2 mM cysteine, 0.5% glucose, and 10 mM sodium fumurate. The stirring was adjusted to 75 rpm, temperature to 30°C, and air bubbling was switched to N_2 bubbling (0.3 L/min). The anaerobic induction proceeded overnight and the next morning the cells were collected using an in-line centrifuge (Eppendorf, 3000 rpm) under N_2 atmosphere. The centrifuge cell was transferred to a glovebox (Coy Laboratories, 3% H_2 atmosphere), the cells were washed with buffer A (50 mM Tris pH 8, 5 mM NaCl, 5% glycerol, 5 mM NaDT), and frozen at -80°C. For purification, all steps were carried out under strict anaerobic conditions with initial cell lysis in a Coy chamber (3% H_2 atmosphere) and subsequent chromatography steps in an Mbraun glove-box (N_2 atmosphere). For cell lysis, 30 μ L Benzonase (Sigma-Aldrich),

lysozyme (Sigma-Aldrich), 2 EDTA-free protease inhibitor tablets dissolved in 1 mL buffer A (Roche), and 2 mM DTT were added to the cell suspension. A microfluidizer (M-110S, Microfluidics) under Ar pressure was used to break the cells. After centrifugation (15,000 rpm, 45 min, 4°C) the cell-free-lysate was first purified over DEAE resin (GE Healthcare) and eluted by a 4 column volume gradient to buffer B (50 mM Tris pH 8, 1M NaCl, 5% glycerol, 5 mM NaDT). Fractions were collected and analyzed for protein content by SDS-PAGE and hydrogenase activity assay (10 mM NaDT, 5 mM methyl viologen) with H₂ evolution measured by GC chromatography (Agilent Technologies). The active fractions were combined and concentrated to ~30 mL using a 30 kDa MWCO membrane and Amicon concentrator cell under Argon gas pressure. The concentrated fraction was purified over 25 mL Strep-Tactin Superflow High Capacity resin (IBA) and eluted into 50 mM Tris pH 8, 200 mM NaCl, 5% glycerol, 5 mM NaDT for the final purification step. Protein concentration was determined by Bradford assay ($\pm 10\%$) using Hemoglobin as the standard, ²⁸ and the H₂ evolution activity (1,700 µmol H₂/min/mg) was measured as described above. FTIR spectroscopy was also used to verify incorporation of the active site H-cluster. Mixtures of CdS NRs and H₂ase were prepared in buffer C (12.5 mM Tris-HCl, 5mM NaCl, 5% glycerol, pH 7) under an anaerobic Ar environment.

2.3 Transient Absorption Spectroscopy. The TA experimental setup was previously described in detail.²⁹ The samples were prepared and sealed under Ar in airtight 2 mm quartz cuvettes. The CdS NR sample concentration was 800 nM. The samples containing both NRs and H_2 as were mixed in 1:1 molar ratios in buffer C. The samples were pumped at 401 nm. The pump beam diameter was 240 μ m and pulse energy was 10 nJ/pulse. The pump power was chosen such that the TA time traces were independent of pump power, indicating that the signal is dominated by NRs with single excitons. The samples were stirred during data collection.

2.4 Light-Driven H₂ Production. Solutions for light-driven H₂ production consisted of 40 nM CdS and 40 nM H₂ase (1:1 molar ratio) with 100 mM ascorbate as a hole scavenger in buffer C in 1.5 mL vials sealed with septa. The samples were illuminated with a 405 nm diode laser (Laserglow Technologies) at 12 mW for 10 min. H₂ was detected in the headspace of the vessel

by injecting a sample of headspace atmosphere into a gas chromatograph (Agilent Technologies 7820A, molecular sieve 5A column, Ar carrier gas, TCD detector).

3. RESULTS

To examine the effect of ligand length on ET kinetics and H₂ production in CdS-H₂ase complexes, CdS NRs with an average diameter of 3.7 ± 0.3 nm and an average length of 22.6 ± 0.3 1.8 nm (Figure S1) were capped with mercaptocarboxylate surface ligands of the form $HS-(CH_2)_n-COO^-$ with n=2,3,5, and 7. These ligands will be referred to by their **n**-value throughout this article. After CdS NR synthesis, the native octadecylphosphonic acid (ODPA) ligands were exchanged with each of these ligands as detailed in the experimental section. The ligand exchange to all of the mercaptocarboxylates causes the band edge absorption to shift 2 nm to the blue, but does not significantly alter the shape of the absorption spectrum (Figure S2 and S3). The blue shift is a signature of the removal of some surface metal ions, which can be displaced as complexes with native ligands during the process of ligand exchange to place thiol ligands on the surface.³⁰⁻³³ The ligand-exchanged particles are soluble in aqueous solutions as the carboxylate end groups are deprotonated at pH 7.34 Photoluminescence (PL) spectra of all samples have similar band-edge and trap emission peak positions and widths, but their relative intensities vary from sample to sample (Figure S4). This implies variations in the excited-state relaxation of the CdS NRs with the different ligands even before coupling with H₂ase. We examine those differences using TA spectroscopy.

3.1 Photoexcited electron relaxation of CdS NRs with varying surface-capping ligands. In order to extract ET kinetics in CdS– H_2 ase complexes, we first address the photoexcited electron relaxation in CdS NRs capped with $\mathbf{n}=2,3,5,7$ mercaptocarboxylate ligands with no enzyme present. The relaxation dynamics of similar CdS NRs have been studied extensively by TA spectroscopy.^{7,8,35-38} These studies provide the background for understanding the effects of the varying surface-capping ligands on CdS NR photophysics, and we describe our results in the context of this prior work. It has been shown that samples of CdS NRs contain structures that are not uniform along the rod length.³⁷ Instead, they contain a wider region, which has been referred to as the "bulb", along the "rod" structure. TA spectra of photoexcited CdS NRs exhibit a transient bleach feature peaked at 457 nm corresponding to the band-edge electron population

(Figure S5). 36,39 Ultrafast (~200 fs) 401 nm pulses excite primarily the rod population. 37 This process is followed by fast (<1 ps) cooling to the band edge. ^{36,39} Photoexcited holes rapidly (~1 ps) trap to the NR surface.^{36,40} After electron cooling, there is a partial decay of the 457 nm peak and a corresponding growth of a broad bleach feature around 479 nm due to electron localization from the rod to the lower energy bulb (Figure S5).^{37,38} The spectral features corresponding to the rod and the bulb are also apparent in the PL spectra (Figure S4), as described previously.³⁷ The timescale (~4 ps) and efficiency (~25%) for electron localization are similar for all four ligands (Figure S6). After this process is complete, the kinetics of the rod and bulb bleach recovery reflect the decay of photoexcited electrons by two pathways: recombination with a trapped hole and electron trapping. 37,38 The rod comprises the vast majority of the particle volume and, given the low enzyme coverage in our study (<1 enzyme per NR), is more relevant for H₂ generation than the minor bulb feature. In Figure S7 we show that the bulb feature kinetics are not noticeably affected by the presence of H₂ase in these samples. For this reason, in the remainder of this manuscript we focus on the electron decay in the rod on the timescale well after electron localization is complete (>100 ps). We take into account the loss of rod population by transfer to the bulb in the calculation of QE_{ET} (see Discussion).

In Figure 1, we examine how the rod electrons decay after the localization process is complete in the CdS NR samples with the different mercaptocarboxylate ligands. We monitor wavelengths on the blue side of the bleach peak in order to reduce the contribution from the 479 nm bulb feature.³⁸ This is important because the bulb feature decays more slowly than the rod, with power-law dynamics at long times, and the contamination from this signal can complicate data analysis.³⁸ The tradeoff for obtaining a more pure rod signal is that the signal-to-noise ratio is lower than it is at the bleach maximum. The rod bleach decay kinetics in Figure 1 vary as a function of ligand, necessitating first an examination of ligand effects on electron relaxation.

As is common in semiconductor nanocrystal samples, ^{41,42} the excited electron decays in Figure 1 are multi-exponential. The complicated dynamics reflect the sample heterogeneity including a variation in the number of electron trapping sites at the nanocrystal surfaces in the ensemble. We analyze the TA decay traces of CdS NRs with different ligands in Figure 1 using a previously described kinetic model that accounts for electron decay by recombination with the trapped hole and by trapping on the nanocrystal surface. Assuming a Poisson distribution in the trap density leads to an expression with only three kinetic parameters: ^{8,35,43,44}

$$S(t) = A \exp[-k_0 t + \langle N_{\rm tr} \rangle (e^{-k_{\rm tr} t} - 1)]. \tag{1}$$

In eq 1, A is a normalization constant, k_0 is the rate constant of recombination, $\langle N_{\rm tr} \rangle$ is the average number of traps in the ensemble, and $k_{\rm tr}$ is the rate constant of electron trapping.

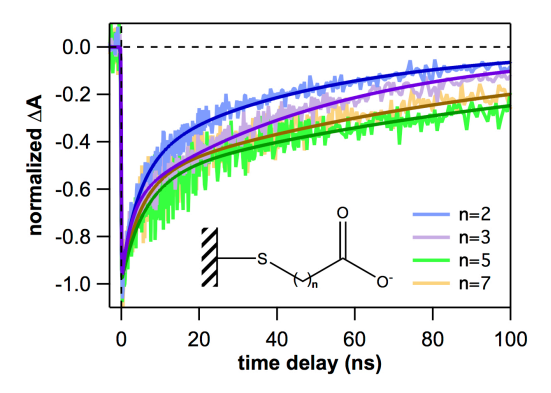


Figure 1. Decays of the rod bleach feature in the TA spectra of CdS NRs with various ligands after 401 nm excitation, normalized at 0.3 ns. Decays of NRs with $\mathbf{n} = 2, 3, 5$, and 7 ligands were monitored at 451 nm, 448 nm, 447 nm and 450 nm, respectively. Corresponding to fits of eq 1 to the data are shown as darker solid lines of the same color. Fit parameters appear in Table S2.

The TA decays of CdS NRs with each of the different mercaptocarboxylate ligands (Figure 1) can be fit well using eq 1 convoluted with the instrument response function. Convolution was carried out using an approximate truncated sum form of eq 1, as described in Section 3.1 of the SI. Fit parameters appear in Table S2. The timescales of electron trapping and recombination are on the order of nanoseconds and tens of nanoseconds, respectively, for these samples. The trap densities are very small ($\langle N_{\rm tr} \rangle \sim 1$) such that recombination dominates the lifetime. Similar results have been reported for CdS nanocrystals previously.^{8,35,42,44} The small number of electron traps suggests effective ligand passivation of the surface cadmium atoms. The values of the decay parameters of CdS NRs with different mercaptocarboxylate ligands all fall within about a factor of two of each other. The fact that all 4 samples can be fit with the same model with only small differences in the resulting parameter values indicates that the photoexcited electrons in CdS NRs with different length ligands decay by the same processes with somewhat different rates. The small differences between the fit parameter values may occur due to variations in surface coverage and ligand packing.

3.2 Kinetics of ET from CdS NRs to H,ase. CdS NRs capped with the n = 2, 3, 5 and 7 mercaptocarboxylate ligands and H2ase were mixed in a 1:1 molar ratio, which has been previously determined to be nearly the optimal ratio for H₂ production in this system.² The TA experiment isolates the one-electron transfer step from CdS NRs to the H₂ase.⁷ Although all the ligands studied have the same functional groups, the differences in aliphatic chain lengths affect ligand hydrophilicity. Increasing ligand length led to decreased colloidal stability of CdS NRs when combined with H₂ase. For this reason, TA data was collected immediately after ligand exchange. Data collection times were limited by the tendency of CdS-H2ase complexes to precipitate after a period of hours, and shorter collection times were required to avoid changes in the sample during the experiment. The duration of the TA experiment for each sample was chosen such that a comparison of absorption spectra before and after data collection confirmed that samples were stable during the experiment (Figure S3). The limits on data collection time also limit the signal-to-noise ratios in the TA data. This is in addition to the signal-to-noise ratio reduction caused by choosing probe wavelengths to the blue of the bleach peak in order to minimize interference from the bulb signal as described above. These limitations on the signalto-noise ratio in the data are responsible for uncertainties in the values of $k_{\rm ET}$, as described later in the text. In Figure 2, the TA kinetics are smoothed to facilitate comparison of the decays with and without the enzyme. Fitting to the kinetic model described below was performed on the raw data.

The addition of H_2 ase introduces ET as an additional pathway by which photoexcited electrons in CdS NRs can decay. As a consequence, the TA bleach feature of CdS NRs with each ligand decays faster in the presence of H_2 ase (Figure 2). For the $\mathbf{n}=3$, and, to a lesser extent, $\mathbf{n}=7$ ligand, the TA kinetic traces do not change dramatically in the presence of H_2 ase, but the differences are statistically significant (Section 3.1 of the SI). Mixing CdS NRs with H_2 ase forms CdS– H_2 ase complexes with a distribution in the number of H_2 ase moieties adsorbed on a given NR, N_{H_2 ase. $^{2.8,45}$ We have previously shown that at low surface coverage, this interaction can be described by a Poisson distribution, characterized by $\langle N_{H_2}\rangle$ as the average number of H_2 ase moieties per nanocrystal available to accept electrons in the ensemble. ET can thus be included in the electron decay kinetic model by introducing an additional decay pathway with rate constant $k_{\rm ET}$ and averaging over the number distribution: $^{8.44,45}$

$$S(t) = A \exp\left[-k_0 t + \langle N_{\rm tr} \rangle (e^{-k_{\rm tr}t} - 1) + \langle N_{\rm H_2 ase} \rangle (e^{-k_{\rm ET}t} - 1)\right]. \tag{2}$$

Analysis and fitting of the data in Figure 2 to eq 2 is detailed in Section 3.1 of the SI. Like eq 1, this equation must be convoluted with the instrument response function in order to account for early time processes. Convolution was carried out using an approximate truncated sum form of eq 2. Fitting of the CdS– H_2 ase decay traces in Figure 2 was performed by fixing the values of k_0 , $\langle N_{\rm tr} \rangle$ and $k_{\rm tr}$ found from fitting free CdS NRs to eq 1 (Figure 1, Table S2), allowing only $\langle N_{\rm H_2 ase} \rangle$ and $k_{\rm ET}$ to vary. This reflects the assumption that the presence of adsorbed H_2 ase does not measurably affect the intrinsic decay pathways of the NRs and only introduces the ET pathway.⁸ To obtain robust estimates of the mean fit parameters and their uncertainties we employed the bootstrapping Monte Carlo method, as detailed in Section 3.1 of the SI.^{8,46} Fits of eq 2 to the CdS– H_2 ase decays are shown in Figure 2 and ET fit parameters and their uncertainties are given in Table 1.

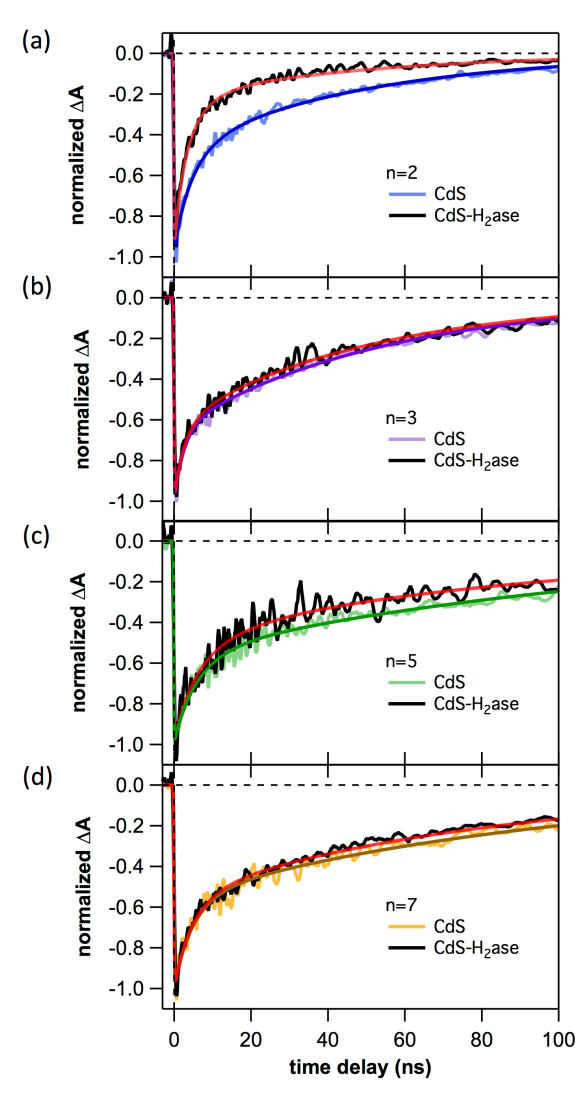


Figure 2. Decay traces of the rod bleach feature in the TA spectra of CdS NRs with and without H_2 as for ligands with (a) $\mathbf{n} = 2$, (b) $\mathbf{n} = 3$, (c) $\mathbf{n} = 5$ and (d) $\mathbf{n} = 7$, excited at 401 nm and normalized at 0.3 ns. Decays of free CdS NRs are reproduced from Figure 1 for each corresponding ligand. CdS- H_2 as decay traces are monitored at the same wavelengths as their corresponding free CdS NR decays from Figure 1. The darker solid lines of the same color as the CdS NRs decays correspond to fits to eq 1, reproduced from Figure 1, while red lines are fits to eq 2 to CdS- H_2 as decays. ET kinetic parameters appear in Table 1.

Table 1. Electron transfer parameters for CdS–H₂ase complexes with varying surface-capping ligands

Ligand	$\langle N_{\rm H_2ase} \rangle$	$k_{\mathrm{ET}}~(\mathrm{s}^{-1})$
$\mathbf{n} = 2$	0.8 ± 0.1	$(1.6 \pm 0.2) \times 10^8$
$\mathbf{n} = 3$	0.10 ± 0.03	$(6\pm2)\times10^7$
$\mathbf{n} = 5$	0.26 ± 0.06	$(3 \pm 2) \times 10^7$
$\mathbf{n} = 7$	0.44 ± 0.06	$(6 \pm 2) \times 10^6$

As plotted in Figure 2, the kinetic data do not appear to have a clear pattern in the rate of ET with ligand length as the lifetime shortening upon the addition of H_2 ase does not seem to change monotonically with ligand. However, fitting to the model of eq 2 allows us to distinguish k_{ET} and the number of H_2 ase moieties bound to determine how each quantity varies with ligand length. Both k_{ET} and $\langle N_{H_2 ase} \rangle$ determine the rate of ET, but they do not have the same ligand dependence. The value of k_{ET} decreases monotonically with increasing ligand length, from 1.6 × 10^8 s⁻¹ for $\mathbf{n} = 2$ to 6×10^6 s⁻¹ for $\mathbf{n} = 7$. The considerable uncertainties of the extracted k_{ET} values are primarily due to the signal-to-noise ratio of the TA decay traces. In contrast to k_{ET} , $\langle N_{H_2 ase} \rangle$, ranging from 0.1 to 0.8, varies for the different ligands with no particular trend. We have already shown in prior work on the $\mathbf{n} = 2$ ligand that the value of $\langle N_{H_2 ase} \rangle$ is somewhat smaller than 1 when the nanorods and enzyme are mixed in 1:1 ratio. Here we observe that the longer ligands have even less H_2 ase adsorbed when mixed at the same ratio.

Figure 3 shows the values of $k_{\rm ET}$ as a function of ligand length. We observe strong distance dependence, with $k_{\rm ET}$ decaying significantly as the ligand length increases. Following the common practice when a bridge length in a donor-bridge-acceptor system is varied, we fit the resulting data points to an exponential decay,

$$k_{\rm ET}(d) = k_{\rm ET}(0)e^{-\beta d},\tag{3}$$

where d is the ligand length in Å, $k_{\rm ET}(0)$ is the rate constant when d=0 (i.e., no ligand between the NR and H₂ase), and β is the electronic decay coefficient describing how $k_{\rm ET}$ decreases with distance. When the data in Figure 3 are fit with eq 3, the resulting value of β is 0.66 ± 0.15 Å⁻¹ and $k_{\rm ET}(0) = (4.8 \pm 3.8) \times 10^9$ s⁻¹. The latter value represents a maximum ET rate constant one can expect to observe in this system in the absence of a ligand. We note, however, that the uncertainty in this value is large because of the uncertainty in the values of $k_{\rm ET}$ (Table 1).

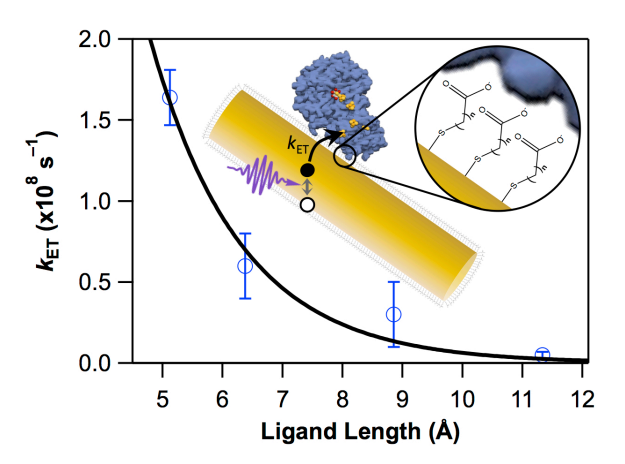


Figure 3. Values of $k_{\rm ET}$ from the TA data as a function of ligand length. The solid black line corresponds to a fit to eq 3. Inset: Schematic depiction of the ET process being measured.

3.3 H_2 production using CdS NRs with varied ligand lengths. Upon illumination with 405 nm light, H_2 production from the CdS- H_2 ase complexes with different ligands in the presence of ascorbate as a sacrificial hole scavenger was measured by gas chromatography (Figure 4). The steps involved in the photochemical H_2 production reaction are shown in Scheme 1. After photon absorption, a photoexcited electron transfers to H_2 ase and is transported to the active site, which binds a proton, resulting in a reduced protonated enzyme (H_2 ase] $^-H^+$). Ascorbate (Asc H^-) is oxidized by the photoexcited hole to form the ascorbyl radical (Asc $^-$) with a release of a proton. This photoexcitation and charge transfer cycle repeats, with the second electron and proton resulting in H_2 generation. The overall reaction is a light-driven oxidation of ascorbate that generates H_2 .

In the measurements of photochemical H_2 production in Figure 4, concentrations of CdS NRs, H_2 ase, and ascorbate, as well as illumination conditions, were the same in all the samples. As in the TA experiments, all samples were mixed in a 1:1 molar ratio and the value of $\langle N_{H_2 ase} \rangle$ may vary between samples. Ascorbate concentrations were in the range where H_2 production no longer depends on the amount of hole scavenger.² Illumination times (10 min) were short compared to the timescale on which these systems become inactivated (hours).² In the absence of H_2 ase, background H_2 production was negligible. Similarly, H_2 was not detectable when the enzyme accepted electrons but the active site was inactivated.⁷ We were able to add the $\mathbf{n} = 10$ ligand to the dataset in this experiment because it was carried out at lower concentrations than TA experiments and the samples were stable with this longer ligand. Figure 4 shows the relative H_2 production as a function of ligand, obtained by dividing the amount of H_2 made by each

sample by the amount of H_2 generated from the $\mathbf{n}=2$ sample. Under the same photoexcitation and concentration conditions for each sample, photochemical H_2 production decreases with increasing ligand length. The data points and error bars indicate the mean and standard deviation from three independent measurements. We have repeated this experiment under a variety conditions, using H_2 as samples with various H_2 evolution activity levels. Although the absolute amounts of H_2 produced vary depending on these conditions, the trend of the relative H_2 production level with ligand is robust. For example, Figure S8 shows a set of H_2 production experiments with different enzyme and nanocrystal batches.

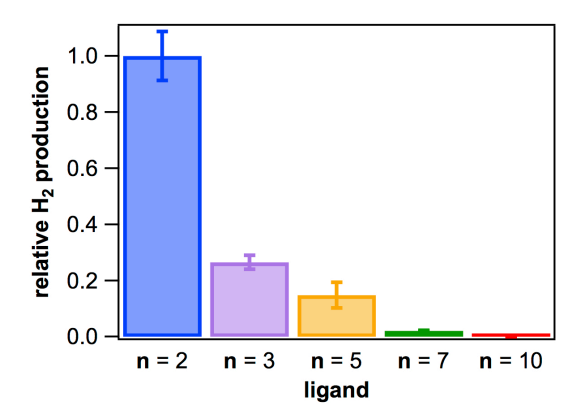
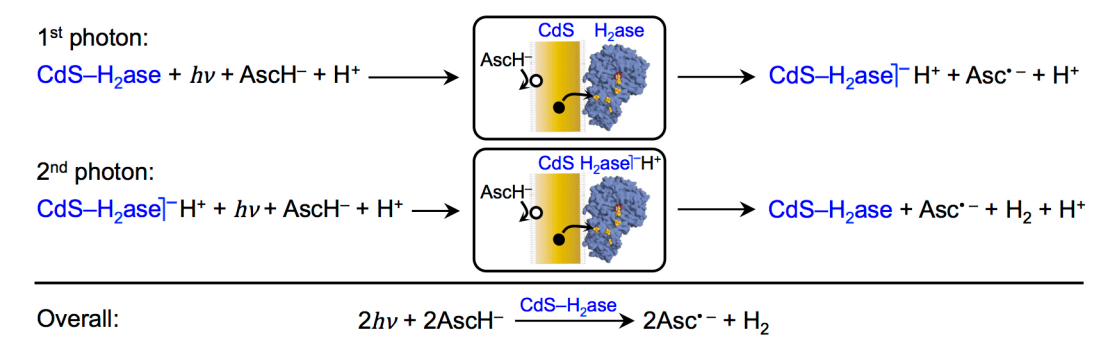


Figure 4: Relative photochemical H₂ production as a function of the ligands capping the CdS surface at equal illumination conditions and concentrations of CdS NRs, H₂ase, and ascorbate.

Scheme 1: Steps involved in the light-driven H₂ production by CdS-H₂ase.



4. DISCUSSION

4.1 Kinetics of ET from CdS NRs to H₂ase. Our investigation of the dependence of ET kinetics on the length of the nanocrystal-surface capping ligand is analogous to several previously reported studies of architectures of the donor-bridge-acceptor type that contain semiconductor

nanocrystals.^{16-25,47,50-52} Many of the donor-bridge-acceptor type systems in which aliphatic molecules form a bridge between the donor and acceptor show exponentially decaying ET rate constants with increasing ligand length due to a decrease in the electronic coupling between the donor and acceptor.^{20,21,23,24} The common interpretation of this result is that the bridge imposes a tunneling barrier for electron transfer. Our data in Figure 3 are consistent with this interpretation.

Our experiments are also somewhat analogous to a study which used protein film cyclic voltammetry and electrochemical scanning tunneling microscopy to measure the catalytic turnover from H₂ase immobilized onto a self-assembled monolayer of mercaptocarboxylates with varying lengths of aliphatic chain on a Au electrode.⁵³ The ligands were the same as the ones used in our study. That work showed a clear exponential decay of turnover frequency with increasing ligand length resulting in an electronic decay constant (β) of 0.82 \pm 0.16 Å⁻¹. From this electrochemical experiment, it was concluded that the catalytic turnover rate was kinetically controlled by ET from the electrode to the enzyme, such that the exponential decay in turnover current is due to the exponential decay in $k_{\rm ET}$. That experiment differs from our work in that it measures a catalytic current directly, does not have a light-driven component with competing kinetic processes but rather direct electron injection from an electrode, and the mercaptocarboxylate molecules are on a flat Au surface rather than curved CdS surface. Nevertheless, the catalytic current is determined by ET rate and its exponential dependence on ligand length is similar to the $k_{\rm ET}$ behavior that we observe in Figure 3. The similarities between our observations and this prior work support our working model of the CdS NR-H₂ase interaction in which the enzyme adsorbs onto the negatively charged layer created by the carboxylate groups, rather than displacing the ligands and adsorbing directly to the nanocrystal surface.² We note that photochemical H₂ production is not equivalent to the electrochemical turnover measurement because photochemical H₂ production depends on the efficiency of ET (i.e., competition between ET and other electron decay pathways in CdS), as discussed below, rather than $k_{\rm ET}$ alone.

While it is clear that the dependence of $k_{\rm ET}$ on ligand length is strong, the values of β and $k_{\rm ET}(0)$ that we report here should be taken as approximate. The value of β , 0.66 ± 0.15 Å⁻¹, falls within the uncertainty range of the value measured by the electrochemical experiments described above. The β value we measure is also close to but smaller than the values of β that have been previously measured for ET through saturated alkyl chains $(0.79-1.2 \text{ Å}^{-1}).^{21,23,54-59}$ However, the

value of β depends on the relative ligand lengths, which may not be accurately represented by a simple model of fully extended molecules. The ligands may not be perfectly aligned and fully extended at all lengths and the different ligands used here may have different packing efficiencies and ordering on the CdS surface. The curvature of the NR surface may also change the molecular structure in a manner that is different for each ligand. All these factors affect the effective values of d, and therefore the value of β . Compared to the literature values, our value of β suggests that the ligands create more compressed nanocrystal-enzyme spacing than fully extended and tightly packed ligand layer would create. The value of $k_{\rm ET}(0)$ depends sensitively on the absolute ligand lengths (both the value of β and the exact meaning of d=0) and thus may be subject to significant systematic error. Our reported value for the maximum ET rate in the CdS- H_2 as system should be taken as an estimate and is probably in the range of 10^9 - 10^{11} s⁻¹.

The strong dependence of the ET rate constant on ligand length provides some guidance for the design of systems that maximize QE_{ET} , which in these systems depends primarily on the ratio of k_{ET} to k_0 . This ratio is already such that QE_{ET} is more than 50% of the maximum in the $\mathbf{n}=2$ system.⁸ A hundred-fold increase in the ratio of k_{ET} to k_0 would maximize QE_{ET} , provided that electron trapping does not become prominent.⁸ The $k_{ET}(0)$ value of 10^9 - 10^{11} s⁻¹ (together with k_0 value of 10^7 s⁻¹) indicates that this can be achieved with the use of very short ligands that place the nanocrystal surface closer to the electron injection site in the enzyme. Since the CdS– H_2 ase complexes rely on the negatively charged surface ligands for solubility, stability, and the electrostatic interaction that mediates binding, ligands cannot be eliminated from the system. However, there have been major developments in the nanocrystal literature specifically concerning ligands that enhance electronic coupling, 63,64 and some of those ligands, provided they are enzyme-compatible, may allow QE_{ET} to be maximized.

4.2 Relationship between ET kinetics and H_2 production. Light-driven H_2 production in the CdS– H_2 ase system is a multi-step process involving light absorption in CdS, ET to H_2 ase, which competes with recombination and trapping, electron transport in the enzyme, and electron donation from ascorbate to CdS.^{2,7,8,13} Since H^+ reduction is a two-electron process, this series of charge transport must happen twice in sequence before a H_2 molecule is released. The fact that the H_2 production trend shown in Figure 4 demonstrates strong ligand-length dependence

suggests that the rate and efficiency of ET play an important role in determining the yield of photodriven H_2 production in the CdS- H_2 ase system. In the case of the $\mathbf{n}=2$ ligand, we have previously shown that the quantum yield of H_2 production is similar to the value of $\mathrm{QE}_{\mathrm{ET}}$, meaning that the majority of electrons transferred to H_2 ase end up in a H_2 molecule. Here, we compare the values of $\mathrm{QE}_{\mathrm{ET}}$ with relative H_2 production for the samples with $\mathbf{n}=2,3,5,$ and 7 ligands. $\mathrm{QE}_{\mathrm{ET}}$ is the fraction of photoexcited electrons that undergo ET in the ensemble rather than decay by processes intrinsic to the CdS NR (i.e., trapping and recombination). In the model of eq 2, the electron population of an individual CdS- H_2 ase complex decays with a total rate of $k_0 + N_{\mathrm{tr}}k_{\mathrm{tr}} + N_{\mathrm{H}_2\mathrm{ase}}k_{\mathrm{ET}}$. The quantum efficiency of electron transfer for the complex with N_{tr} electron traps and $N_{\mathrm{H}_2\mathrm{ase}}$ bound H_2 ase moieties is $N_{\mathrm{H}_2\mathrm{ase}}k_{\mathrm{ET}}/(k_0 + N_{\mathrm{tr}}k_{\mathrm{tr}} + N_{\mathrm{H}_2\mathrm{ase}}k_{\mathrm{ET}})$. The total $\mathrm{QE}_{\mathrm{ET}}$ of the ensemble is found by summing over the Poisson distributions in both the number of electron traps and H_2 ase moieties bound (eq 4):

$$QE_{ET} = \sum_{N_{H_{2}ase}=0}^{\infty} \sum_{N_{tr}=0}^{\infty} \frac{\langle N_{H_{2}ase} \rangle^{N_{H_{2}ase}} e^{-\langle N_{H_{2}ase} \rangle}}{N_{H_{2}ase}!} \frac{\langle N_{tr} \rangle^{N_{tr}} e^{-\langle N_{tr} \rangle}}{N_{tr}!} \frac{N_{H_{2}ase} k_{ET}}{k_{0} + N_{tr} k_{tr} + N_{H_{2}ase} k_{ET}}.$$
(4)

Because we assume that non-uniform CdS NRs do not contribute to ET or H₂-production at the low mixing ratios used here, QE_{ET} was adjusted for the fraction of structures in which the electron localizes to the bulb (Figure S6). Equation 4, after accounting for this adjustment, was used to calculate the QE_{ET} for each ligand using the model parameters listed in Table 1 and Table S2. Note that these values of QE_{ET} are calculated using the measured values of $\langle N_{\rm H_2 ase} \rangle$, which vary among ligands at the 1:1 mixing ratio of CdS NRs to H₂ase. The resulting QE_{ET} values for each ligand, along with relative H₂ production, normalized so that the two match for the $\bf n$ = 2 ligand, are plotted in Figure 5.

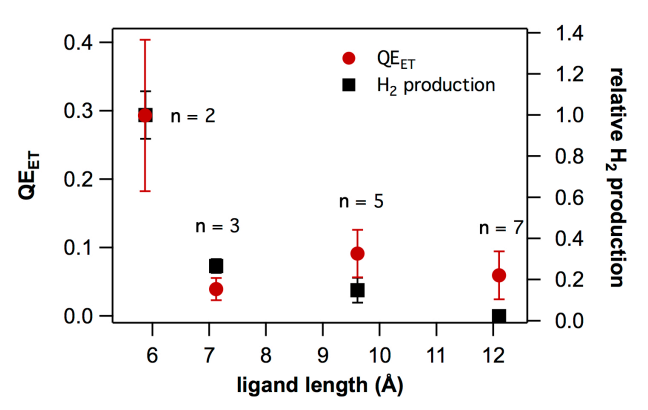


Figure 5: QE_{ET} and relative H_2 production as a function of ligand length. Error bars on QE_{ET} values come from error propagation of all input parameters from Table 1 and Table S2 and their uncertainties. Relative H_2 production values are normalized to match the QE_{ET} for the $\mathbf{n}=2$ ligand.

The strong dependence and the rapid decay of QE_{ET} with ligand length in Figure 5 is a consequence of both the decreasing value of k_{ET} and the changes in the value of $\langle N_{\rm H_2 ase} \rangle$, which is highest for the ${\bf n}=2$ sample. It is not clear why the enzyme binding varies from ligand to ligand even though the NRs and ${\bf H_2}$ as are always mixed in a 1:1 ratio. We suspect that the differences in the chemical environment (dipole moment, ligand orientation, ligand packing and coverage, etc.) create a complex interplay of factors that contribute to the $\langle N_{\rm H_2 ase} \rangle$ values we measure. The trend of relative ${\bf H_2}$ production as a function of ligand length is qualitatively similar to that of the ${\bf QE}_{\rm ET}$ (Figure 5). This similarity suggests that the combination of both decreasing $k_{\rm ET}$ and varying $\langle N_{\rm H_2 ase} \rangle$ when ligand length changes is also at play in the ${\bf H_2}$ -production experiments. The implication of this result is that the control and enhancement of ${\bf H_2}$ -production efficiency will require the increase in $k_{\rm ET}$ as well as control and enhancement of nanocrystal-enzyme binding. We note that, in the hypothetical scenario where each sample in Figure 5 were to have the same value of $\langle N_{\rm H_2 ase} \rangle$, ${\bf QE}_{\rm ET}$ would have a much weaker dependence on ligand length (Figure S9).

Our results support the idea that, although there are multiple steps in H₂ production by CdS–H₂ase complexes, ET is a critical step determining overall photochemical efficiency. This is true provided that sufficient hole scavenger is present and hole removal keeps up with ET.⁶⁵⁻⁶⁷ In systems where ET to the catalyst is fast, such as CdS-Pt, the hole scavenging rate limits the overall H₂ production efficiency.^{67,68} In the CdS-H₂ase system, where ET is slower by orders of

magnitude, it is easier to reach a regime where hole scavenging is not limiting the overall photochemical activity. We have previously shown that H₂ production in this system depends on ascorbate concentration but reaches a saturation limit where this dependence becomes flat.² In the H₂ production data in Figure 4, the ascorbate concentration is well past that limit, making ET the key step that determines the overall H₂ production efficiency. The enzyme is excellent at utilizing the electrons it receives from the nanocrystals over a broad range of excitation intensities.^{2,7,8} Under the conditions where ET is the efficiency-limiting step for photochemical H₂ production, the key to maximizing the output of the system is in controlling the ratio of ET rate and the rates of the competing relaxation pathways, as described above, as well as nanocrystal-enzyme binding, both of which can be achieved with judicious choice of surface-capping ligands.

5. CONCLUSIONS

We have studied the effect of mercaptocarboxylate surface ligands of various lengths on CdS NR excited state dynamics, ET to hydrogenase, and photochemical H_2 production. Rate constants for ET decrease exponentially with ligand length, as observed in other donor-bridge-acceptor systems involving nanocrystals. Quantum efficiencies of ET depend on both $k_{\rm ET}$ and the number of enzymes adsorbed, both of which vary with ligand. H_2 production closely tracks the trends in $QE_{\rm ET}$, demonstrating the critical role of surface-capping ligands in the photochemical activity of these systems. Our results suggest that using shorter ligands could lead to significant increases in the rate of ET, which would maximize $QE_{\rm ET}$ of this system and enhance photochemical H_2 generation.

ASSOCIATED CONTENT

Supporting Information. Nanocrystal characterization (TEM, absorption and fluorescence spectroscopy), TA spectra, fitting and error analysis, reproducibility of H₂ production trend, quantum efficiency of electron transfer.

AUTHOR INFORMATION

Corresponding Author

*gordana.dukovic@colorado.edu

Present Addresses

§Department of Chemistry, Luther College, Decorah, Iowa 52101 ⊥ Office of Water, US Environmental Protection Agency, Washington DC 20460

ACKNOWLEDGMENTS

Nanocrystal synthesis, characterization, TA spectroscopy, and kinetic modeling were supported by the U.S. Department of Energy, Office of Basic Energy Sciences, Division of Materials Sciences and Engineering under Award DE-SC0010334. J.K.U. acknowledges support from National Science Foundation Graduate Research Fellowships under Grant No. DGE 1144083. S.G. acknowledges support from the Kolenkow-Reitz Fellowship from Carleton College. Hydrogenase synthesis and purification were supported by the U.S. Department of Energy, Office of Basic Energy Sciences, Division of Chemical Sciences, Geosciences, and Biosciences; and the U.S. Department of Energy under Contract No. DE-AC36-08-GO28308 with the National Renewable Energy. We thank Joel Eaves for helpful discussions.

REFERENCES

- (1) Brown, K. A.; Dayal, S.; Ai, X.; Rumbles, G.; King, P. W. Controlled Assembly of Hydrogenase-CdTe Nanocrystal Hybrids for Solar Hydrogen Production. *J Am Chem Soc* **2010**, *132*, 9672-9680.
- (2) Brown, K. A.; Wilker, M. B.; Boehm, M.; Dukovic, G.; King, P. W. Characterization of Photochemical Processes for H2 Production by CdS Nanorod-[FeFe] Hydrogenase Complexes. *J Am Chem Soc* **2012**, *134*, 5627-5636.
- (3) Chaudhary, Y. S.; Woolerton, T. W.; Allen, C. S.; Warner, J. H.; Pierce, E.; Ragsdale, S. W.; Armstrong, F. A. Visible Light-Driven CO2 Reduction by Enzyme Coupled CdS Nanocrystals. *Chem Commun* **2012**, *48*, 58-60.
- (4) Greene, B. L.; Joseph, C. A.; Maroney, M. J.; Dyer, R. B. Direct Evidence of Active-Site Reduction and Photodriven Catalysis in Sensitized Hydrogenase Assemblies. *J Am Chem Soc* **2012**, *134*, 11108-11111.
- (5) Burai, T. N.; Panay, A. J.; Zhu, H. M.; Lian, T. Q.; Lutz, S. Light-Driven, Quantum Dot-Mediated Regeneration of FMN To Drive Reduction of Ketoisophorone by Old Yellow Enzyme. *Acs Catal* **2012**, *2*, 667-670.
- (6) Brown, K. A.; Song, Q.; Mulder, D. W.; King, P. W. Diameter Dependent Electron Transfer Kinetics in Semiconductor-Enzyme Complexes. *ACS Nano* **2014**, *8*, 10790-10798.
- (7) Wilker, M. B.; Shinopoulos, K. E.; Brown, K. A.; Mulder, D. W.; King, P. W.; Dukovic, G. Electron Transfer Kinetics in CdS Nanorod-[FeFe]-Hydrogenase Complexes and Implications for Photochemical H2 Generation. *J Am Chem Soc* **2014**, *136*, 4316-4324.

- (8) Utterback, J. K.; Wilker, M. B.; Brown, K. A.; King, P. W.; Eaves, J. D.; Dukovic, G. Competition between Electron Transfer, Trapping, and Recombination in CdS Nanorod-Hydrogenase Complexes. *Phys Chem Chem Phys* **2015**, *17*, 5538-5542.
- (9) Sakimoto, K. K.; Wong, A. B.; Yang, P. Self-Photosensitization of Nonphotosynthetic bacteria for Solar-to-Chemical Production. *Science* **2016**, *351*, 74-77.
- (10) Brown, K. A.; Wilker, M. B.; Boehm, M.; Hamby, H.; Dukovic, G.; King, P. W. Photocatalytic Regeneration of Nicotinamide Cofactors by Quantum Dot–Enzyme Biohybrid Complexes. *Acs Catal* **2016**, *6*, 2201-2204.
- (11) Brown, K. A.; Harris, D. F.; Wilker, M. B.; Rasmussen, A.; Khadka, N.; Hamby, H.; Keable, S.; Dukovic, G.; Peters, J. W.; Seefeldt, L. C.et al Light-Driven Dinitrogen Reduction Catalyzed by a CdS:Nitrogenase MoFe Protein Biohybrid. *Science* **2016**, *352*, 448-450.
- (12) Kornienko, N.; Sakimoto, K. K.; Herlihy, D. M.; Nguyen, S. C.; Alivisatos, A. P.; Harris, C. B.; Schwartzberg, A.; Yang, P. Spectroscopic Elucidation of Energy Transfer in Hybrid Inorganic–Biological Organisms for Solar-to-Chemical Production. *Proc. Natl. Acad. Sci. U. S. A.* **2016**, *113*, 11750-11755.
- (13) Simon, T.; Carlson, M. T.; Stolarczyk, J. K.; Feldmann, J. Electron Transfer Rate vs Recombination Losses in Photocatalytic H2 Generation on Pt-Decorated CdS Nanorods. *Acs Energy Lett* **2016**, *1*, 1137-1142.
- (14) Ratzloff, M. W.; Wilker, M. B.; Mulder, D. W.; Lubner, C. E.; Hamby, H.; Brown, K. A.; Dukovic, G.; King, P. W. Activation Thermodynamics and H/D Kinetic Isotope Effect of the Hox to HredH+ Transition in [FeFe] Hydrogenase. *J Am Chem Soc* **2017**, *139*, 12879-12882.
- (15) Peterson, M. D.; Cass, L. C.; Harris, R. D.; Edme, K.; Sung, K.; Weiss, E. A. The Role of Ligands in Determining the Exciton Relaxation Dynamics in Semiconductor Quantum Dots. *Annu. Rev. Phys. Chem.* **2014**, *65*, 317-339.
- (16) Lawless, D.; Kapoor, S.; Meisel, D. Bifunctional Capping of CdS Nanoparticles and Bridging to TiO2. *J. Phys. Chem.* **1995**, *99*, 10329-10335.
- (17) Bakkers, E. P. A. M.; Roest, A. L.; Marsman, A. W.; Jenneskens, L. W.; de Jong-van Steensel, L. I.; Kelly, J. J.; Vanmaekelbergh, D. Characterization of Photoinduced Electron Tunneling in Gold/SAM/Q-CdSe Systems by Time-Resolved Photoelectrochemistry. *J. Phys. Chem. B* **2000**, *104*, 7266-7272.
- (18) Adams, D. M.; Brus, L.; Chidsey, C. E. D.; Creager, S.; Creutz, C.; Kagan, C. R.; Kamat, P. V.; Lieberman, M.; Lindsay, S.; Marcus, R. A.et al Charge Transfer on the Nanoscale: Current Status. *J Phys Chem B* **2003**, *107*, 6668-6697.
- (19) Dibbell, R. S.; Youker, D. G.; Watson, D. F. Excited-State Electron Transfer from CdS Quantum Dots to TiO2 Nanoparticles via Molecular Linkers with Phenylene Bridges. *J. Phys. Chem. C* **2009**, *113*, 18643-18651.
- (20) Dibbell, R. S.; Watson, D. F. Distance-Dependent Electron Transfer in Tethered Assemblies of CdS Quantum Dots and TiO2 Nanoparticles. *J Phys Chem C* **2009**, *113*, 3139-3149.
- (21) Tagliazucchi, M.; Tice, D. B.; Sweeney, C. M.; Morris-Cohen, A. J.; Weiss, E. A. Ligand-Controlled Rates of Photoinduced Electron Transfer in Hybrid CdSe Nanocrystal/Poly(viologen) Films. *ACS Nano* **2011**, *5*, 9907-9917.
- (22) Hyun, B. R.; Bartnik, A. C.; Sun, L. F.; Hanrath, T.; Wise, F. W. Control of Electron Transfer from Lead-Salt Nanocrystals to TiO2. *Nano Lett* **2011**, *11*, 2126-2132.

- (23) Wang, H.; McNellis, E. R.; Kinge, S.; Bonn, M.; Canovas, E. Tuning Electron Transfer Rates through Molecular Bridges in Quantum Dot Sensitized Oxides. *Nano Lett* **2013**, *13*, 5311-5315.
- (24) Hines, D. A.; Forrest, R. P.; Corcelli, S. A.; Kamat, P. V. Predicting the Rate Constant of Electron Tunneling Reactions at the CdSe–TiO2 Interface. *J Phys Chem B* **2015**, *119*, 7439-7446.
- (25) Ding, T. X.; Olshansky, J. H.; Leone, S. R.; Alivisatos, A. P. Efficiency of Hole Transfer from Photoexcited Quantum Dots to Covalently Linked Molecular Species. *J Am Chem Soc* **2015**, *137*, 2021-2029.
- (26) Carbone, L.; Nobile, C.; De Giorgi, M.; Sala, F. D.; Morello, G.; Pompa, P.; Hytch, M.; Snoeck, E.; Fiore, A.; Franchini, I. R.et al Synthesis and Micrometer-Scale Assembly of Colloidal CdSe/CdS Nanorods prepared by a Seeded Growth Approach. *Nano Lett* **2007**, *7*, 2942-2950.
- (27) King, P. W.; Posewitz, M. C.; Ghirardi, M. L.; Seibert, M. Functional Studies of [FeFe] Hydrogenase Maturation in an Escherichia coli Biosynthetic System. *J Bacteriol* **2006**, *188*, 2163-2172.
- (28) Bradford, M. M. Rapid and Sensitive Method for Quantitation of Microgram Quantities of Protein Utilizing Principle of Protein-Dye Binding. *Anal Biochem* **1976**, *72*, 248-254.
- (29) Tseng, H. W.; Wilker, M. B.; Damrauer, N. H.; Dukovic, G. Charge Transfer Dynamics between Photoexcited CdS Nanorods and Mononuclear Ru Water-Oxidation Catalysts. *J Am Chem Soc* **2013**, *135*, 3383-3386.
- (30) Anderson, N. C.; Hendricks, M. P.; Choi, J. J.; Owen, J. S. Ligand Exchange and the Stoichiometry of Metal Chalcogenide Nanocrystals: Spectroscopic Observation of Facile Metal-Carboxylate Displacement and Binding. *J Am Chem Soc* **2013**, *135*, 18536-18548.
- (31) Goodwin, E. D.; Diroll, B. T.; Oh, S. J.; Paik, T.; Murray, C. B.; Kagan, C. R. Effects of Post-Synthesis Processing on CdSe Nanocrystals and Their Solids: Correlation between Surface Chemistry and Optoelectronic Properties. *J Phys Chem C* **2014**, *118*, 27097-27105.
- (32) Shakeri, B.; Meulenberg, R. W. A Closer Look into the Traditional Purification Process of CdSe Semiconductor Quantum Dots. *Langmuir* **2015**, *31*, 13433-13440.
- (33) Knauf, R. R.; Lennox, J. C.; Dempsey, J. L. Quantifying Ligand Exchange Reactions at CdSe Nanocrystal Surfaces. *Chem Mater* **2016**, *28*, 4762-4770.
- (34) Dai, Z.; Ju, H. Effect of Chain Length on the Surface Properties of [omega]-Carboxy Alkanethiol Self-Assembled Monolayers. *Phys Chem Chem Phys* **2001**, *3*, 3769-3773.
- (35) Sadhu, S.; Patra, A. Relaxation Dynamics of Anisotropic Shaped CdS Nanoparticles. *J Phys Chem C* **2011**, *115*, 16867-16872.
- (36) Wu, K. F.; Zhu, H. M.; Liu, Z.; Rodriguez-Cordoba, W.; Lian, T. Q. Ultrafast Charge Separation and Long-Lived Charge Separated State in Photocatalytic CdS-Pt Nanorod Heterostructures. *J Am Chem Soc* **2012**, *134*, 10337-10340.
- (37) Wu, K.; Rodríguez-Córdoba, W.; Lian, T. Exciton Localization and Dissociation Dynamics in CdS and CdS–Pt Quantum Confined Nanorods: Effect of Nonuniform Rod Diameters. *J Phys Chem B* **2014**, *118*, 14062-14069.
- (38) Utterback, J. K.; Grennell, A. N.; Wilker, M. B.; Pearce, O. M.; Eaves, J. D.; Dukovic, G. Observation of Trapped-Hole Diffusion on the Surfaces of CdS Nanorods. *Nat Chem* **2016**, 8, 1061-1066.
- (39) Klimov, V. I. Spectral and Dynamical Properties of Multilexcitons in Semiconductor Nanocrystals. *Annu Rev Phys Chem* **2007**, *58*, 635-673.

- (40) Klimov, V. I.; Schwarz, C. J.; McBranch, D. W.; Leatherdale, C. A.; Bawendi, M. G. Ultrafast Dynamics of Inter- and Intraband Transitions in Semiconductor Nanocrystals: Implications for Quantum-Dot Lasers. *Phys Rev B* **1999**, *60*, R2177-R2180.
- (41) Jones, M.; Scholes, G. D. On the use of Time-Resolved Photoluminescence as a Probe of Nanocrystal Photoexcitation Dynamics. *J Mater Chem* **2010**, *20*, 3533-3538.
- (42) Knowles, K. E.; McArthur, E. A.; Weiss, E. A. A Multi-Timescale Map of Radiative and Nonradiative Decay Pathways for Excitons in CdSe Quantum Dots. *ACS Nano* **2011**, *5*, 2026-2035.
- (43) Tachiya, M. Application of a Generating Function to Reaction-Kinetics in Micelles Kinetics of Quenching of Luminescent Probes in Micelles. *Chem Phys Lett* **1975**, *33*, 289-292.
- (44) Sadhu, S.; Tachiya, M.; Patra, A. A Stochastic Model for Energy Transfer from CdS Quantum Dots/Rods (Donors) to Nile Red Dye (Acceptors). *J. Phys. Chem. C* **2009**, *113*, 19488-19492.
- (45) Leng, H. X.; Loy, J.; Amin, V.; Weiss, E. A.; Pelton, M. Electron Transfer from Single Semiconductor Nanocrystals to Individual Acceptor Molecules. *Acs Energy Lett* **2016**, *1*, 9-15.
- (46) Press, W. H.; Teukolsky, S. A.; Vetterling, W. T.; Flannery, B. P.: *Numerical Recipes: The Art of Scientific Computing*; 3rd ed.; Cambridge University Press: Cambridge, 2007.
- (47) Anderson, N. A.; Lian, T. Q. Ultrafast Electron Transfer at the Molecule-Semiconductor Nanoparticle Interface. *Annu Rev Phys Chem* **2005**, *56*, 491-519.
- (48) Ratzloff, M. W.; Wilker, M. B.; Mulder, D. W.; Lubner, C. E.; Hamby, H.; Brown, K. A.; Dukovic, G.; King, P. W. Activation Thermodynamics and H/D Kinetic Isotope Effect of the Hox to HredH+ Transition in [FeFe] Hydrogenase. *J. Am. Chem. Soc.* **2017**, *139*, 12879-12882.
- (49) Warren, J. J.; Mayer, J. M. Tuning of the Thermochemical and Kinetic Properties of Ascorbate by Its Local Environment: Solution Chemistry and Biochemical Implications. *J Am Chem Soc* **2010**, *132*, 7784-7793.
- (50) Pernik, D. R.; Tvrdy, K.; Radich, J. G.; Kamat, P. V. Tracking the Adsorption and Electron Injection Rates of CdSe Quantum Dots on TiO2: Linked versus Direct Attachment. *J Phys Chem C* **2011**, *115*, 13511-13519.
- (51) Knowles, K. E.; Peterson, M. D.; McPhail, M. R.; Weiss, E. A. Exciton Dissociation within Quantum Dot-Organic Complexes: Mechanisms, Use as a Probe of Interfacial Structure, and Applications. *J Phys Chem C* **2013**, *117*, 10229-10243.
- (52) Bakkers, E. P. A. M.; Marsman, A. W.; Jenneskens, L. W.; Vanmaekelbergh, D. Distance-Dependent Electron Transfer in Au/Spacer/Q-CdSe Assemblies. *Angew. Chem. Int. Edit.* **2000**, *39*, 2297-2299.
- (53) Madden, C.; Vaughn, M. D.; Díez-Pérez, I.; Brown, K. A.; King, P. W.; Gust, D.; Moore, A. L.; Moore, T. A. Catalytic Turnover of [FeFe]-Hydrogenase Based on Single-Molecule Imaging. *J Am Chem Soc* **2012**, *134*, 1577-1582.
- (54) Wold, D. J.; Haag, R.; Rampi, M. A.; Frisbie, C. D. Distance Dependence of Electron Tunneling through Self-Assembled Monolayers measured by Conducting Probe Atomic Force Microscopy: Unsaturated versus Saturated Molecular Junctions. *J Phys Chem B* **2002**, *106*, 2813-2816.
- (55) Smalley, J. F.; Finklea, H. O.; Chidsey, C. E. D.; Linford, M. R.; Creager, S. E.; Ferraris, J. P.; Chalfant, K.; Zawodzinsk, T.; Feldberg, S. W.; Newton, M. D. Heterogeneous Electron-Transfer Kinetics for Ruthenium and Ferrocene Redox Moieties through Alkanethiol Monolayers on Gold. *J Am Chem Soc* **2003**, *125*, 2004-2013.

- (56) Holmlin, R. E.; Haag, R.; Chabinyc, M. L.; Ismagilov, R. F.; Cohen, A. E.; Terfort, A.; Rampi, M. A.; Whitesides, G. M. Electron Transport through Thin Organic Films in Metal-Insulator-Metal Junctions based on Self-Assembled Monolayers. *J Am Chem Soc* **2001**, *123*, 5075-5085.
- (57) Bumm, L. A.; Arnold, J. J.; Dunbar, T. D.; Allara, D. L.; Weiss, P. S. Electron Transfer through Organic Molecules. *J Phys Chem B* **1999**, *103*, 8122-8127.
- (58) Weber, K.; Hockett, L.; Creager, S. Long-range Electronic Coupling between Ferrocene and Gold in Alkanethiolate-Based Monolayers on Electrodes. *J Phys Chem B* **1997**, *101*, 8286-8291.
- (59) Wang, W.; Lee, T.; Reed, M. A. Elastic and Inelastic Electron Tunneling in Alkane Self-Assembled Monolayers. *J Phys Chem B* **2004**, *108*, 18398-18407.
- (60) Hostetler, M. J.; Stokes, J. J.; Murray, R. W. Infrared Spectroscopy of Three-Dimensional Self-Assembled Monolayers: N-alkanethiolate Monolayers on Gold Cluster Compounds. *Langmuir* **1996**, *12*, 3604-3612.
- (61) Ghorai, P. K.; Glotzer, S. C. Molecular Dynamics Simulation Study of Self-Assembled Monolayers of Alkanethiol Surfactants on Spherical Gold Nanoparticles. *J Phys Chem C* **2007**, *111*, 15857-15862.
- (62) Love, C. J.; Estroff, L. A.; Kriebel, J. K.; Nuzzo, R. G.; Whitesides, G. M. Self-Assembled Monolayers of Thiolates on Metals as a Form of Nanotechnology. *Chem. Rev.* **2005**, *105*, 1103-1169.
- (63) Brutchey, R. L.; Hens, Z.; Kovalenko, M. V.: Surface Chemistry of Colloidal Semiconductor Nanocrystals: Organic, Inorganic and Hybrid. In *Chemistry of Organo-Hybrids: Synthesis and Characterization of Functional Nano-Objects*; Charleux, B., Coperet, C., Lacote, E., Eds.; John Wiley & Sons: New York, 2015.
- (64) Harris, R. D.; Homan, S. B.; Mohamad, K.; He, C.; Nepomnyashchii, A. B.; Swenson, N. K.; Lian, S.; Calzada, R.; Weiss, E. A. Electronic Processes within Quantum Dot-Molecule Complexes. *Chem. Rev.* **2016**, *116*, 12865-12919.
- (65) Berr, M. J.; Wagner, P.; Fischbach, S.; Vaneski, A.; Schneider, J.; Susha, A. S.; Rogach, A. L.; Jackel, F.; Feldmann, J. Hole Scavenger Redox Potentials Determine Quantum Efficiency and Stability of Pt-Decorated CdS Nanorods for Photocatalytic Hydrogen Generation. *Appl Phys Lett* **2012**, *100*, 223903.
- (66) Simon, T.; Bouchonville, N.; Berr, M. J.; Vaneski, A.; Adrovic, A.; Volbers, D.; Wyrwich, R.; Doblinger, M.; Susha, A. S.; Rogach, A. L.et al Redox Shuttle Mechanism Enhances Photocatalytic H2 Generation on Ni-Decorated CdS Nanorods. *Nat Mater* **2014**, *13*, 1013-1018.
- (67) Wu, K. F.; Chen, Z. Y.; Lv, H. J.; Zhu, H. M.; Hill, C. L.; Lian, T. Q. Hole Removal Rate Limits Photodriven H2 Generation Efficiency in CdS-Pt and CdSe/CdS-Pt Semiconductor Nanorod-Metal Tip Heterostructures. *J Am Chem Soc* **2014**, *136*, 7708-7716.
- (68) Berr, M. J.; Vaneski, A.; Mauser, C.; Fischbach, S.; Susha, A. S.; Rogach, A. L.; Jackel, F.; Feldmann, J. Delayed Photoelectron Transfer in Pt-Decorated CdS Nanorods under Hydrogen Generation Conditions. *Small* **2012**, *8*, 291-297.

TOC Graphic:

